The Astrophysical Journal, 890:72 (11pp), 2020 February 10 https://doi.org/10.3847/1538-4357/ab698e

Optical Variability of the TeV Blazar 1ES 0806+524 on Diverse Timescales

Ashwani Pandey[1,2,14], Alok C. Gupta[1], Sofia O. Kurtanidze[3,4,5], Paul J. Wiita[6], G. Damljanovic[7], R. Bachev[8], Jin Zhang[9], O. M. Kurtanidze[3,4,10,11], A. Darriba[12,13], R. A. Chigladze[3,5], G. Latev[8], M. G. Nikolashvili[3,4], S. Peneva[8], E. Semkov[8], A. Strigachev[8], S. N. Tiwari[2], and O. Vince[7]

[1] Aryabhatta Research Institute of Observational Sciences (ARIES), Manora Peak, Nainital 263002, India; ashwanitapan@gmail.com
[2] Department of Physics, DDU Gorakhpur University, Gorakhpur 273009, India
[3] Abastumani Observatory, Mt. Kanobili, 0301 Abastumani, Georgia
[4] Zentrum für Astronomie der Universität Heidelberg, Landessternwarte, Königstuhl 12, D-69117 Heidelberg, Germany
[5] Samtskhe-Javakheti State University, Rustaveli Str. 113, 0080 Akhaltsikhe, Georgia
[6] Department of Physics, The College of New Jersey, 2000 Pennington Rd., Ewing, NJ 08628-0718, USA
[7] Astronomical Observatory, Volgina 7, 11060 Belgrade, Serbia
[8] Institute of Astronomy and National Astronomical Observatory, Bulgarian Academy of Sciences, 72 Tsarigradsko Shosse Boulevard, 1784 Sofia, Bulgaria
[9] Key Laboratory of Space Astronomy and Technology, National Astronomical Observatories, Chinese Academy of Sciences, Beijing 100012, People's Republic of China
[10] Engelhardt Astronomical Observatory, Kazan Federal University, Tatarstan, Russia
[11] Center for Astrophysics, Guangzhou University, Guangzhou 510006, People's Republic of China
[12] American Association of Variable Star Observers (AAVSO), 49 Bay State Road, Cambridge, MA 02138, USA
[13] Group M1, Centro Astronómico de Avila, Madrid, Spain
Received 2019 November 20; revised 2020 January 1; accepted 2020 January 7; published 2020 February 13

Abstract

We report the results of our optical (*VRI*) photometric observations of the TeV blazar 1ES 0806+524 on 153 nights during 2011–2019 using seven optical telescopes in Europe and Asia. We investigated the variability of the blazar on intraday as well as on long-term timescales. We examined 18 intraday light curves for flux and color variations using the most reliable power-enhanced *F*-test and the nested ANOVA test. Only on one night was a small, but significant, variation found, in both *V*-band and *R*-band light curves. The $V-R$ color index was constant on every one of those nights. Flux density changes of around 80% were seen over the course of these eight years in multiple bands. We found a weighted mean optical spectral index of 0.639 ± 0.002 during our monitoring period by fitting a power law ($F_\nu \propto \nu^{-\alpha}$) in 23 optical (*VRI*) spectral energy distributions of 1ES 0806+524. We discuss different possible mechanisms responsible for blazar variability on diverse timescales.

Unified Astronomy Thesaurus concepts: Active galactic nuclei (16); Blazars (164); Observational astronomy (1145); CCD photometry (208); Radio loud quasars (1349); Active galaxies (17); Optical observation (1169); Relativistic jets (1390); Optical telescopes (1174); BL Lacertae objects (158)

1. Introduction

Active galactic nuclei (AGNs) are universally believed to be powered by accreting supermassive black holes ($\geqslant 10^6\ M_\odot$) lying at their centers (Rees 1984). About 10%–15% of AGNs clearly include two well-collimated jets of relativistic particles and are known as jetted-AGNs (Padovani et al. 2017). These relativistic jets are particularly luminous at radio and γ-ray frequencies. The different jetted-AGNs are distinguished by their viewing angles with respect to the observer's line of sight, with blazars being those in which the relativistic jets are aligned at very small ($\leqslant 15°$–$20°$) viewing angles (Urry & Padovani 1995). Blazars are further divided into BL Lacertae objects ($EW^{15}_{rest} < 5$ Å) and flat-spectrum radio quasars (FSRQs; $EW_{rest} > 5$ Å) on the basis of the strength of emission lines in their optical/ultraviolet spectra (e.g., Stocke et al. 1991; Marcha et al. 1996). Their nonthermal broadband spectral energy distributions (SEDs) have a characteristic double bump structures (e.g., Fossati et al. 1998). The low-frequency component, which peaks in infrared to X-ray frequencies, is well interpreted as synchrotron emission from the relativistic electrons in the jet. Based on the rest-frame synchrotron peak frequency (ν^S_{peak}), Abdo et al. (2010) classified blazars as low-synchrotron-peaked blazars (LSPs; $\nu^S_{peak} \leqslant 10^{14}$ Hz), intermediate-synchrotron-peaked blazars (ISPs; 10^{14} Hz $< \nu^S_{peak} < 10^{15}$ Hz), and high-synchrotron-peaked blazars (HSPs; $\nu^S_{peak} \geqslant 10^{15}$ Hz). The high-frequency component peaks at GeV energies in LSPs (including FSRQs and low-frequency-peaked BL Lac objects (LBLs)) and at TeV energies in HSPs or high-frequency-peaked BL Lac objects (HBLs). The physical origin of the high-frequency component is still debated (e.g., Böttcher 2007).

Blazars are known for their highly variable nature on diverse timescales. On the basis of variability timescales (t_{var}), blazar variability can be broadly classified as: intraday variability (IDV) or microvariability ($t_{var} \sim$ less than a day), short-term variability (STV; $t_{var} \sim$ few days to few months) and long-term variability (LTV; $t_{var} \sim$ several months to years). Optical variability in the light curves (LCs) of blazars has been studied extensively on all these three timescales by several authors (e.g., Miller et al. 1989; Carini 1990; Wagner & Witzel 1995; Gupta et al. 2004, 2016, and references therein). Optical observations of blazars reveal that color changes are often observed together with flux variations. BL Lac objects are found to follow a bluer-when-brighter (BWB) color trend, while a redder-when-brighter (RWB) color behavior is usually seen in FSRQs (e.g., Wu et al. 2012; Wierzcholska et al. 2015).

The AGN 1ES 0806+524 ($\alpha_{2000} = 08^h09^m49\overset{s}{.}2$; $\delta_{2000} = +52°18'58\overset{''}{.}4$; $z = 0.138$ Bade et al. 1998) was classified as a

[14] Corresponding author.
[15] Rest-frame equivalent width.

Table 1
Details of Telescopes and Instruments Used

Code	A	B	C	D	E	F	G
Telescope	1.3 m DFOT	1.04 m ST	60 cm AO	1.4 m ASV	70 cm	50/70 cm NAO	35.6 cm C14 XLT
CCD model	Andor 2K	PyLoN	FLI PL9000	Andor iKon-L	Apogee Ap6E	FLI PL16803	ATIK 383L+ Monochrome
Chip size (pixels)	2048 × 2048	1340 × 1300	3056 × 3056	2048 × 2048	1024 × 1024	4096 × 4096	3354 × 2529
Scale (arcsec/pixel)	0.535	0.305	1.0	0.244	2.4	1.079	1.38
Field (arcmin^2)	18 × 18	6.8 × 6.6	17 × 17	8.3 × 8.3	15 × 15	73.66 × 73.66	25.46 × 19.16
Gain (e^-/ADU)	2.0	4.0	1.0	1.0	8.0	1.0	1.8
Read-out noise (e^-rms)	7.0	6.4	9.0	7.0	14.0	9.0	7.0
Typical seeing (arcsec)	1.2–2.0	1.2–2.1	2.0–3.0	1.0–1.5	1.0–2.0	2.0–4.0	1.3–2.0

Note. A: 1.3 m Devasthal Fast Optical Telescope (DFOT) at ARIES, Nainital, India. B: 1.04 m Sampuranand Telescope at ARIES, Nainital, India. C: 60 cm Cassegrain telescope at Astronomical Observatory (AO) Belogradchik, Bulgaria. D: 1.4 m telescope at Astronomical Station Vidojevica (ASV), Serbia. E: 70 cm meniscus telescope at Abastumani Observatory, Georgia. F: 50/70 cm Schmidt telescope at National Astronomical Observatory (NAO), Rozhen, Bulgaria. G: 35.6 cm Celestron C14 XLT telescope at Las Casqueras, Spain.

BL Lac object on the basis of its featureless optical spectra (Schachter et al. 1993). It was first detected at very high energy ($E > 300$ GeV) γ−ray in 2008 by the Very Energetic Radiation Imaging Telescope Array System (Acciari et al. 2009). Optical R-band observations of 1ES 0806+524 were carried out from 1997 December 27 to 2006 May 30 by Kurtanidze et al. (2009). During this period it was detected in the brightest state of $R = 14.81$ on 2004 September 13, while the faintest magnitude observed was $R = 15.69$ on 1999 on April 7 and the maximum brightness variation was $\Delta R = 0.88$. Gopal-Krishna et al. (2011) monitored this blazar on four nights but did not find IDV on any night. Quasi-simultaneous multicolor observations of 1ES 0806+524 were performed from 2005 December to 2011 February by Man et al. (2014) and they found a strong BWB trend on long timescales, but no variation on IDV timescales.

The key motivation of this paper is to study the multiband optical flux and spectral variability properties of the TeV blazar 1ES 0806+524 on diverse timescales. We present the first extensive multiband optical photometric observations of the blazar in V, R, and I bands from 2011 January 25 to 2019 April 12 using seven optical telescopes. We investigated the flux and spectral variability properties on intraday and longer timescales. We also extracted optical SEDs of the blazar during the observing period.

The paper is organized as follows: Section 2 gives details of observation and data reduction procedures; Section 3 describes the analysis techniques we used. Results of our variability analysis are given in Section 4, while Section 5 presents a discussion. Finally, a summary of our results is given in Section 6.

2. Observations and Data Reduction

We performed optical photometric observations of the TeV blazar 1ES 0806+524 from 2011 January 25 to 2019 April 12. Our observations were carried out using a total of seven ground-based telescopes; two in India, two in Bulgaria, one in Georgia, one in Serbia, and one in Spain. We observed the blazar for 153 nights during which a total of 2263 image frames were collected in V, R, and I optical bands. The technical details of the telescopes and the instruments used for observations are given in Table 1. The complete observation log of the optical photometric observations of the TeV HBL 1ES 0806+524 is given in Table 2.

We monitored the blazar 1ES 0806+524 for a total of 10 nights between 2016 December 30 and 2018 December 29 with two Ritchey−Chretien Cassegrain reflector telescopes in India: the 1.3 m ($f/4$) Devasthal Fast Optical Telescope and 1.04 m ($f/13$) Sampuranand Telescope (ST). Both of these telescopes are equipped with Johnson–Cousins *UBVRI* filters. Using these telescopes, we observed the blazar quasi-simultaneously in V and R optical filters for ∼3–4 hr during each observing night. Single I-band image frames were also taken on each night. The cleaning (bias-subtraction, flat-fielding and cosmic-ray removal) of the raw CCD images was done using IRAF.[16] We then performed aperture photometry in each cleaned CCD image using DAOPHOT[17] II software to get the instrumental magnitudes of the blazar and the stars in the image frame. Details of the data reduction process are given in Pandey et al. (2019).

Observations with the 60 cm Cassegrain telescope located at the Astronomical Observatory Belogradchik, Bulgaria, were carried out in optical V, R, and I bands for a total of 13 nights between 2011 January 25 and 2015 December 14. We also observed the source quasi-simultaneously in V and R bands on 2019 March 28 with the 50/70 cm Schmidt telescope at the National Astronomical Observatory, Rozhen, Bulgaria. The data reduction process for these telescopes is explained in detail in Gaur et al. (2012a).

Optical photometric observations of 1ES 0806+524 were conducted in the R-band from 2016 January 18 to 2018 April 23 for a total of 66 nights using the 70 cm ($f/3$) Meniscus telescope located at Abastumani Observatory, Georgia. The telescope is equipped with an Apogee CCD camera AP6E and Cousins R filter. Cleaning of the raw data was done using IRAF and the photometry was performed using DAOPHOT II.

Quasi-simultaneous monitoring of the source in V and R filters was also performed using the 1.4 m telescope located at Astronomical Station Vidojevica, Serbia. The telescope has a CCD camera Andor iKon-L and is equipped with Johnson–Cousins *UBVRI* broadband filters. With this telescope, we observed the blazar for a total of nine nights between 2018 December 2 and 2019 April 7. The optical photometric data analysis procedure we followed is given in Gupta et al. (2019).

We also carried out optical V-band observations of the TeV blazar 1ES 0806+524 on 54 nights between 2016 August 19 and 2019 April 12 using a Celestron C14 XLT 35.6 cm

[16] Image Reduction and Analysis Facility (IRAF) is distributed by the National Optical Astronomy Observatory, which is operated by the Association of Universities for Research in Astronomy (AURA) under a cooperative agreement with the National Science Foundation.
[17] Dominion Astronomical Observatory Photometry.

Table 2
Observation Log for the TeV blazar 1ES 0806+524

Observation date	Telescope	Data points	Observation date	Telescope	Data points	Observation date	Telescope	Data points
		V, R,I			*V, R,I*			*V, R,I*
2011 Jan 25	C	1, 1, 1	2017 Feb 24	G	1, 0, 0	2018 Jan 17	E	0, 4, 0
2011 Feb 6	C	1, 1, 1	2017 Feb 24	G	1, 0, 0	2018 Jan 20	G	1, 0, 0
2011 Feb 7	C	1, 1, 1	2017 Feb 28	E	0, 4, 0	2018 Jan 27	G	1, 0, 0
2011 May 27	C	1, 1, 1	2017 Mar 5	E	0, 4, 0	2018 Feb 1	E	0, 3, 0
2012 Apr 10	C	1, 1, 1	2017 Mar 10	G	1, 0, 0	2018 Feb 2	G	1, 0, 0
2012 Apr 12	C	1, 1, 1	2017 Mar 11	G	1, 0, 0	2018 Feb 8	B	25, 25, 1
2012 May 12	C	1, 1, 1	2017 Mar 14	E	0, 4, 0	2018 Feb 9	B	25, 25, 1
2015 Feb 12	C	1, 1, 1	2017 Mar 17	G	1, 0, 0	2018 Feb 10	G	1, 0, 0
2015 Feb 13	C	1, 1, 1	2017 Mar 18	G	1, 0, 0	2018 Feb 14	E	0, 4, 0
2015 Apr 19	C	0, 1, 1	2017 Mar 19	E	0, 4, 0	2018 Feb 17	G	1, 0, 0
2015 Apr 22	C	0, 1, 1	2017 Mar 19	G	1, 0, 0	2018 Feb 21	A	30, 30, 1
2015 Apr 25	C	0, 1, 1	2017 Mar 28	E	0, 5, 0	2018 Feb 24	G	1, 0, 0
2015 Dec 14	C	0, 1, 1	2017 Apr 1	E	0, 4, 0	2018 Feb 25	G	1, 0, 0
2016 Jan 18	E	0, 3, 0	2017 Apr 1	G	1, 0, 0	2018 Feb 26	E	0, 3, 0
2016 Feb 2	E	0, 4, 0	2017 Apr 7	G	1, 0, 0	2018 Mar 10	G	1, 0, 0
2016 Feb 3	E	0, 4, 0	2017 Apr 8	G	1, 0, 0	2018 Mar 12	E	0, 7, 0
2016 Feb 19	E	0, 6, 0	2017 Apr 10	E	0, 5, 0	2018 Mar 24	G	1, 0, 0
2016 Feb 29	E	0, 4, 0	2017 Apr 15	E	0, 6, 0	2018 Mar 31	G	1, 0, 0
2016 Mar 18	E	0, 4, 0	2017 Apr 21	G	1, 0, 0	2018 Apr 4	E	0, 4, 0
2016 Mar 30	E	0, 6, 0	2017 Apr 25	E	0, 4, 0	2018 Apr 9	E	0, 4, 0
2016 Apr 3	E	0, 4, 0	2017 Apr 28	G	1, 0, 0	2018 Apr 14	G	1, 0, 0
2016 Apr 11	E	0, 4, 0	2017 Apr 30	E	0, 5, 0	2018 Apr 15	E	0, 4, 0
2016 Apr 17	E	0, 8, 0	2017 May 12	E	0, 4, 0	2018 Apr 23	E	0, 4, 0
2016 May 1	E	0, 4, 0	2017 May 22	E	0, 8, 0	2018 Apr 29	G	1, 0, 0
2016 Aug 19	G	1, 0, 0	2017 May 26	G	1, 0, 0	2018 Apr 30	G	1, 0, 0
2016 Aug 23	E	0, 2, 0	2017 Jun 8	E	0, 3, 0	2018 May 4	G	1, 0, 0
2016 Aug 30	E	0, 4, 0	2017 Jun 9	G	1, 0, 0	2018 May 12	G	1, 0, 0
2016 Sep 18	E	0, 2, 0	2017 Jun 16	G	1, 0, 0	2018 May 14	G	1, 0, 0
2016 Oct 2	E	0, 3, 0	2017 Jun 23	E	0, 4, 0	2018 Jun 15	G	1, 0, 0
2016 Oct 3	E	0, 5, 0	2017 Jul 3	E	0, 5, 0	2018 Nov 17	G	1, 0, 0
2016 Oct 12	E	0, 5, 0	2017 Aug 29	E	0, 4, 0	2018 Dec 2	D	3, 3, 3
2016 Nov 8	E	0, 5, 0	2017 Sep 4	E	0, 4, 0	2018 Dec 15	A	30, 30, 1
2016 Nov 13	E	0, 6, 0	2017 Sep 12	E	0, 4, 0	2018 Dec 16	A	41, 41, 1
2016 Nov 22	E	0, 4, 0	2017 Sep 17	E	0, 4, 0	2018 Dec 28	A	34, 34, 1
2016 Nov 26	E	0, 4, 0	2017 Sep 17	G	1, 0, 0	2018 Dec 29	A	33, 33, 1
2016 Dec 6	E	0, 5, 0	2017 Sep 28	G	1, 0, 0	2018 Dec 29	G	1, 0, 0
2016 Dec 8	E	0, 4, 0	2017 Sep 29	G	1, 0, 0	2019 Jan 25	G	1, 0, 0
2016 Dec 10	G	1, 0, 0	2017 Oct 12	G	1, 0, 0	2019 Feb 16	G	1, 0, 0
2016 Dec 21	E	0, 6, 0	2017 Oct 14	E	0, 4, 0	2019 Feb 22	G	1, 0, 0
2016 Dec 30	A	37, 37, 1	2017 Oct 22	G	1, 0, 0	2019 Feb 28	D	94, 94, 1
2017 Jan 3	E	0, 5, 0	2017 Oct 24	E	0, 4, 0	2019 Mar 6	D	84, 84, 0
2017 Jan 6	E	0, 4, 0	2017 Oct 28	G	1, 0, 0	2019 Mar 9	D	17, 17, 0
2017 Jan 13	G	1, 0, 0	2017 Nov 11	E	0, 4, 0	2019 Mar 9	G	1, 0, 0
2017 Jan 14	G	1, 0, 0	2017 Nov 19	G	1, 0, 0	2019 Mar 12	D	67, 67, 1
2017 Jan 17	E	0, 4, 0	2017 Nov 21	E	0, 6, 0	2019 Mar 15	G	1, 0, 0
2017 Jan 19	A	27, 27, 1	2017 Nov 26	E	0, 4, 0	2019 Mar 28	F	61, 61, 0
2017 Feb 2	E	0, 6, 0	2017 Dec 9	E	0, 4, 0	2019 Mar 29	D	22, 22, 0
2017 Feb 13	E	0, 4, 0	2017 Dec 16	G	1, 0, 0	2019 Mar 30	D	138, 138, 0
2017 Feb 17	G	1, 0, 0	2017 Dec 19	E	0, 4, 0	2019 Apr 6	D	58, 58, 1
2017 Feb 18	G	1, 0, 0	2018 Jan 2	E	0, 6, 0	2019 Apr 7	D	1, 1, 0
2017 Feb 19	E	0, 4, 0	2018 Jan 10	B	20, 20, 1	2019 Apr 12	G	1, 0, 0

telescope at Las Casqueras, Spain. The CCD raw images were cleaned using the standard process and photometry was done using MaxIm DL software.

The instrumental magnitudes of the blazar were calibrated using the standard star C4, taken from the blazar finding chart,[18] having brightness close to that of the blazar.

We monitored the TeV HBL 1ES 0806+524 for a total of 153 nights in optical *V*, *R*, and *I* bands during our campaign. Out of these 153 nights, 85 had multiple observations made of the source in a specific filter. However, to search for IDV flux and spectral variations, we only selected nights in which at least 15 measurements were taken in an optical band by a telescope. By applying this criterion, 18 nights qualified for the IDV flux and spectral variability analysis; those nights with more than 15 observations had data taken in the *V* and *R* bands.

[18] https://www.lsw.uni-heidelberg.de/projects/extragalactic/charts/0806+526.html

3. Analysis Techniques

To search for intraday variations in the optical LCs of 1ES 0806 +524, we used two powerful statistical tests that have frequently been employed recently to examine AGN variability; the power-enhanced F-test and the nested analysis of variance (ANOVA) test (de Diego 2014; de Diego et al. 2015). In both tests, multiple field stars are involved as comparison stars in the analysis to produce a more reliable result. A large enough number of independent observations that allowed us to properly look for IDV were made on 18 nights between 30 December 2016 and 6 April 2019.

3.1. Power-enhanced F-test

In the power-enhanced F-test, the brightest unsaturated star is used as a reference star to get the differential LCs (DLCs) of the blazar and the other comparison stars (Gaur et al. 2015; Poleđnikova et al. 2016; Kshama et al. 2017). This statistical test is explained in detail in Pandey et al. (2019). First, we estimated the variance, $s^2_{\rm blz}$, of the blazar DLCs. We then calculated the combined variance, s^2_c, of the DLCs of all the comparison stars using Equation (2) of Pandey et al. (2019). The value of power-enhanced F-statistics, F_{enh}, is calculated as

$$F_{enh} = \frac{s^2_{\rm blz}}{s^2_c}, \quad (1)$$

In this work, we always observed three or more stars that were close in magnitude to the blazar and were in its field. Out of these nearby stars, we selected the brightest star as the reference star and the remaining (k) field stars as the comparison stars. Since the blazar and all the comparison stars are in the same field, they have the same number of observations (N). We estimated the critical value (F_c) of F-statistics at $\alpha = 0.01$ (i.e., at nominal 99% confidence level) using the number of degrees of freedom in the numerator, $\nu_{\rm blz} = N - 1$ and in denominator, $\nu_c = k(N-1)$. We then compared the F_{enh} value with the critical value (F_c). An LC is considered variable (V) if $F_{enh} \geqslant F_c$; otherwise, we label it nonvariable (NV).

3.2. Nested ANOVA

In the nested ANOVA test, all the comparison stars are used as reference stars to get the DLCs of the AGN (de Diego et al. 2015; Pandey et al. 2019). These different DLCs of a blazar are then grouped such that each group has five points. The F statistic is calculated as $F = {\rm MS}_G/{\rm MS}_{O(G)}$, where ${\rm MS}_G$ and ${\rm MS}_{O(G)}$, calculated using Equation (4) of de Diego et al. (2015), are the mean square due to groups and the mean square due to nested observations in groups, respectively. An LC is called variable (V) if the $F-$statistic $\geqslant (F_c)$ at $\alpha = 0.01$, otherwise NV.

The results of both the statistical tests are given in Table 3, where an LC is conservatively labeled as variable (V) only if both the tests found significant variations in it, otherwise it is labeled as NV, though of course there may be weak intrinsic variability even in some of those cases.

3.3. Intraday Variability Amplitude

We calculated the amplitude (A, in percent) of flux and color variations on both IDV and LTV timescales using the following equation (Heidt & Wagner 1996):

$$A = 100 \times \sqrt{(A_{\rm max} - A_{\rm min})^2 - 2\sigma^2}, \quad (2)$$

where $A_{\rm max}$ and $A_{\rm min}$ denote the maximum and minimum calibrated magnitudes, respectively, in the LC of the blazar, and σ represents the mean error.

4. Results

4.1. Variability on IDV Timescale

4.1.1. Flux Variability

The calibrated optical IDV LCs of the TeV blazar 1ES 0806 +524 in V and R bands are plotted in the upper panel of each plot in Figure 1. As can been seen, all the IDV LCs are either flat or exhibit quite small fluctuations.

We examined the V- and R-band LCs of 1ES 0806+524 on the 18 nights with dense sampling for intraday variations using the two very reliable tests discussed above. The results of the analysis are given in Table 3. We found no IDV that was statistically significant by both tests on any night except on 2018 January 10. The amplitude of variations in the V- and R-band LCs on 2018 January 10, calculated using Equation (2), are only 3.5% and 3.9%, respectively. There were 11 more occasions when the source showed IDV by the nested ANOVA test but did not show IDV by the power-enhanced F-test, so we did not consider those nights as definitely possessing IDV.

4.1.2. Spectral Variability

To study spectral variability of the blazar 1ES 0806+524 on IDV timescales, the $V-R$ color indices (CIs) were calculated for each pair of V and R magnitudes and are plotted against time (color–time) in the bottom panels of Figure 1.

We then examined the color–time plots using the two statistical tests discussed in Sections 3.1 and 3.2. The results of the analysis are also shown in Table 3. We found no significant temporal variations in $V-R$ CIs on IDV timescales.

4.2. Variability on LTV Timescale

4.2.1. Flux Variability

The LTV-calibrated LCs of the blazar 1ES 0806+524 in V, R, and I bands for the entire observing period are plotted in Figure 2, where the daily averaged calibrated magnitudes are plotted against time. We have shifted the V- and I-band LCs by +0.5 and −0.5 mag, respectively, to make the long-term optical variability patterns more easily visible. Variations on LTV timescales can be clearly seen in all three optical LCs. The amplitudes of variation in V, R, and I optical wavebands are 84.3%, 81.6%, and 76.5%, respectively. The average magnitudes in V, R, and I bands were 15.45, 15.06, and 14.51, respectively. During our eight year long observing campaign, the blazar 1ES 0806+524 was detected in the brightest state of $R_{\rm mag} = 14.53$ on 2011 February 6, while the faintest magnitude observed was $R_{\rm mag} = 15.35$ on 2019 March 6. Our brightest and faintest magnitudes of 1ES 0806+524 are very close to previous observations of this blazar. Aleksić et al. (2015) observed the blazar in the brightest state of $R_{\rm mag} = 14.38$ and Reinthal et al. (2012) reported the faintest state of $R_{\rm mag} = 15.27$.

Table 3
Results of IDV Analysis of 1ES 0806+524

Observation date	Band	Power-enhanced F-test			Nested ANOVA			Status	Amplitude
		DoF(ν_1,ν_2)	F_{enh}	F_c	DoF(ν_1,ν_2)	F	F_c		%
2016 Dec 30	*V*	36, 108	0.66	1.81	6, 28	3.83	3.53	NV	⋯
	R	36, 108	0.50	1.81	6, 28	2.21	3.53	NV	⋯
	V–R	36, 108	0.61	1.81	6, 28	1.96	3.53	NV	⋯
2017 Jan 19	*V*	26, 78	0.47	2.00	4, 20	1.91	4.43	NV	⋯
	R	26, 78	0.41	2.00	4, 20	1.32	4.43	NV	⋯
	V–R	26, 78	0.80	2.00	4, 20	2.44	4.43	NV	⋯
2018 Jan 10	*V*	19, 38	2.81	2.42	3, 16	14.27	5.29	V	3.46
	R	19, 38	3.08	2.42	3, 16	27.56	5.29	V	3.88
	V–R	19, 38	0.44	2.42	3, 16	0.37	5.29	NV	⋯
2018 Feb 8	*V*	24, 48	0.85	2.20	4, 20	14.89	4.43	NV	⋯
	R	24, 48	0.70	2.20	4, 20	13.09	4.43	NV	⋯
	V–R	24, 48	0.67	2.20	4, 20	1.10	4.43	NV	⋯
2018 Feb 9	*V*	24, 48	0.84	2.20	4, 20	3.11	4.43	NV	⋯
	R	24, 48	0.71	2.20	4, 20	0.98	4.43	NV	⋯
	V–R	24, 48	0.96	2.20	4, 20	0.35	4.43	NV	⋯
2018 Feb 21	*V*	29, 87	0.59	1.94	5, 24	1.58	3.90	NV	⋯
	R	29, 87	0.62	1.94	5, 24	1.99	3.90	NV	⋯
	V–R	29, 87	1.33	1.94	5, 24	1.49	3.90	NV	⋯
2018 Dec 15	*V*	29, 87	0.57	1.94	5, 24	3.00	3.90	NV	⋯
	R	29, 87	0.54	1.94	5, 24	4.97	3.90	NV	⋯
	V–R	29, 87	1.31	1.94	5, 24	0.55	3.90	NV	⋯
2018 Dec 16	*V*	40, 120	0.56	1.76	7, 32	1.98	3.26	NV	⋯
	R	40, 120	0.49	1.76	7, 32	2.44	3.26	NV	⋯
	V–R	40, 120	0.88	1.76	7, 32	0.58	3.26	NV	⋯
2018 Dec 28	*V*	33, 99	1.20	1.86	5, 24	5.11	3.90	NV	⋯
	R	33, 99	1.04	1.86	5, 24	7.23	3.90	NV	⋯
	V–R	33, 99	0.88	1.86	5, 24	2.27	3.90	NV	⋯
2018 Dec 29	*V*	32, 96	0.77	1.88	5, 24	0.99	3.90	NV	⋯
	R	32, 96	0.22	1.88	5, 24	0.49	3.90	NV	⋯
	V–R	32, 96	0.68	1.88	5, 24	1.27	3.90	NV	⋯
2019 Feb 28	*V*	93, 279	1.96	1.46	17, 72	2.14	2.23	NV	⋯
	R	93, 279	1.75	1.46	17, 72	0.55	2.23	NV	⋯
	V–R	90, 270	1.52	1.47	17, 72	1.64	2.23	NV	⋯
2019 Mar 6	*V*	83, 166	1.07	1.54	15, 64	2.46	2.33	NV	⋯
	R	83, 166	0.80	1.54	15, 64	3.63	2.33	NV	⋯
	V–R	83, 166	0.79	1.54	15, 64	2.28	2.33	NV	⋯
2019 Mar 9	*V*	16, 32	1.37	2.62	2, 12	0.80	6.93	NV	⋯
	R	16, 32	0.97	2.62	2, 12	0.08	6.93	NV	⋯
	V–R	16, 32	0.92	2.62	2, 12	0.15	6.93	NV	⋯
2019 Mar 12	*V*	66, 198	1.51	1.56	12, 52	3.18	2.55	NV	⋯
	R	66, 198	1.26	1.56	12, 52	5.55	2.55	NV	⋯
	V–R	64, 192	1.18	1.57	12, 52	0.98	2.55	NV	⋯
2019 Mar 28	*V*	60, 180	0.95	1.60	11, 48	2.06	2.64	NV	⋯
	R	60, 180	0.77	1.60	11, 48	0.65	2.64	NV	⋯
	V–R	60, 180	0.85	1.60	11, 48	1.53	2.64	NV	⋯
2019 Mar 29	*V*	21, 63	1.02	2.16	3, 16	1.94	5.29	NV	⋯
	R	21, 63	0.76	2.16	3, 16	2.34	5.29	NV	⋯
	V–R	21, 63	0.80	2.16	3, 16	6.50	5.29	NV	⋯
2019 Mar 30	*V*	137, 274	1.02	1.40	26, 108	0.96	1.93	NV	⋯
	R	137, 274	0.99	1.40	26, 108	0.60	1.93	NV	⋯
	V–R	137, 274	0.99	1.40	26, 108	0.51	1.93	NV	⋯
2019 Apr 6	*V*	57, 171	1.65	1.61	10, 44	1.13	2.75	NV	⋯
	R	57, 171	0.97	1.61	10, 44	2.23	2.75	NV	⋯
	V–R	55, 165	0.94	1.63	10, 44	1.90	2.75	NV	⋯

4.2.2. Spectral Variability

To investigate possible spectral changes over longer timescales, we plot optical CIs, both with respect to time and *R*-band magnitude, which has a relatively large overlap with other bands, in Figures 3 and 4, respectively. Visual inspection of both figures shows clear color variations. However, to check whether these variations are systematic or not, we fitted each panel in Figures 3 and 4 with a straight line of the form $Y = mX + c$. The results of the fit for color–time and color–magnitude plots are given in Tables 4 and 5, respectively. Only the $R - I$ color shows a significant systematic variation with time, while systematic color variations with respect to R magnitude are found in $V - I$ and $R - I$ colors.

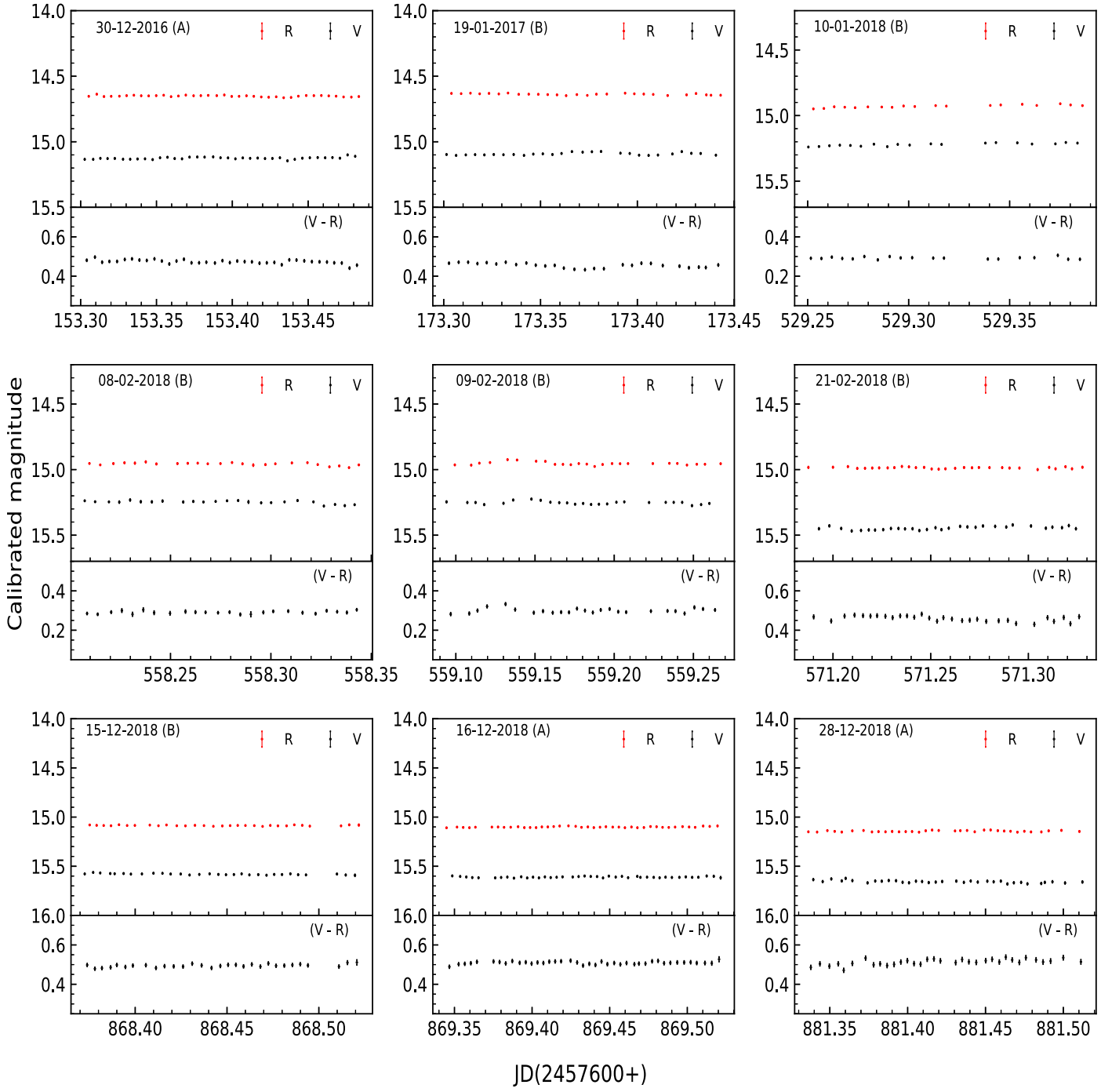

Figure 1. Optical IDV light curves (LCs) of the TeV HBL 1ES 0806+524. The observation date and the telescope code are given in each plot. Top panel: *V*- and *R*-band LCs. Bottom panel: variation of $V-R$ color with time.

4.3. Spectral Energy Distribution

For a detailed study of spectral variations on longer timescales, we extracted the optical (*VRI*) SEDs of 1ES 0806 +524 for those nights in which observations were taken in all three optical bands. For this, we first subtracted the Galactic extinction, A_λ, taken from the NASA Extragalactic Database[19] from the calibrated magnitudes and then converted it into extinction-corrected flux densities, F_ν. The optical SEDs of 1ES 0806+524, in $\log(F_\nu) - \log(\nu)$ representation, are shown in Figure 5. Since the optical continuum spectra of blazars are usually well represented by a simple power law ($F_\nu \propto \nu^{-\alpha}$, α being the optical spectral index), we fitted each SED with a straight line ($\log(F_\nu) = -\alpha \log(\nu) + C$) to obtain the optical spectral indices of the blazar. The results of linear fits are given in Table 6. The derived spectral indices range from 0.469 ± 0.027 to 0.905 ± 0.183, quantifying the obvious spectral variation in the optical band. However, the errors in some of the spectral indices are very large. The weighted mean optical spectral index of 1ES 0806+524 during our observation campaign was 0.639 ± 0.002, which is similar to those found by Gaur et al. (2012b). The behavior of optical spectral indices

[19] https://ned.ipac.caltech.edu/

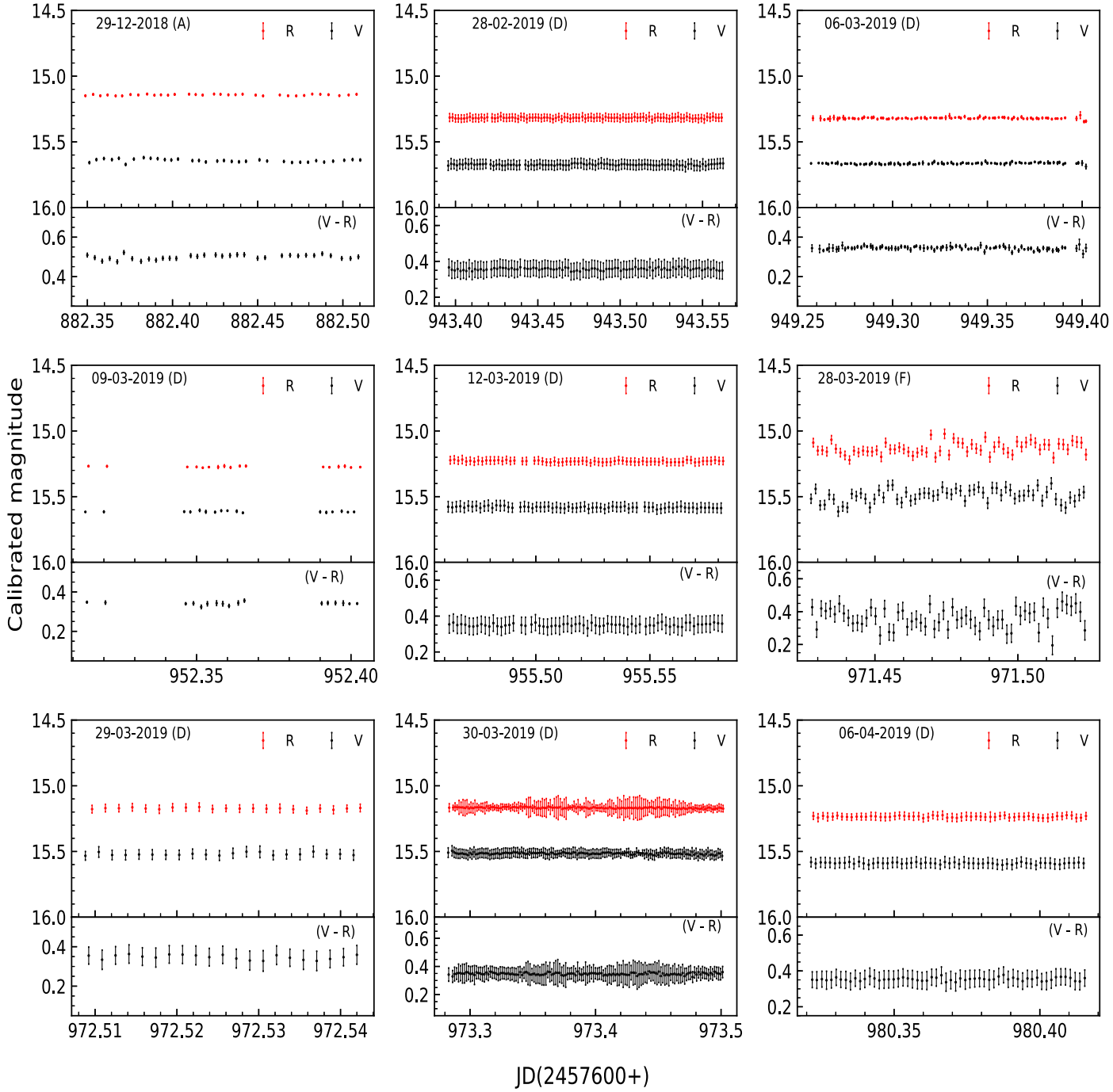

Figure 1. (Continued.)

is often studied with respect to time and *V*-band magnitude (e.g., Gupta et al. 2019 and references therein). So we plotted the spectral indices with respect to time and *V*-band magnitude in the top and bottom panels of Figure 6, respectively. To search for any systematic variations in the spectral index, we fitted each panel in Figure 6 with a straight line. The results of the fits are given in Table 7. No systematic temporal variation is found in the optical spectral index. The spectral index shows a significant positive correlation with *V*-band magnitude, indicating a BWB behavior. We also investigated the variation of spectral indices with respect to *R*-band magnitude and *I*-band magnitude and found similar trends.

5. Discussion

Flux variability on diverse timescales at all electromagnetic bands is an important characteristic of blazars. It is a powerful tool to better understand the geometry of the emitting regions and the different underlying emission mechanisms (e.g., Ciprini et al. 2003). Blazars belong to the jetted subclass of AGNs, and have one of their relativistic jets pointing close to the observer. The nonthermal relativistic jet emission from a blazar is, therefore, highly Doppler-boosted. The Doppler-boosted non-thermal jet emission generally swamps out the thermal emission from the accretion disk (AD) feeding the supermassive black

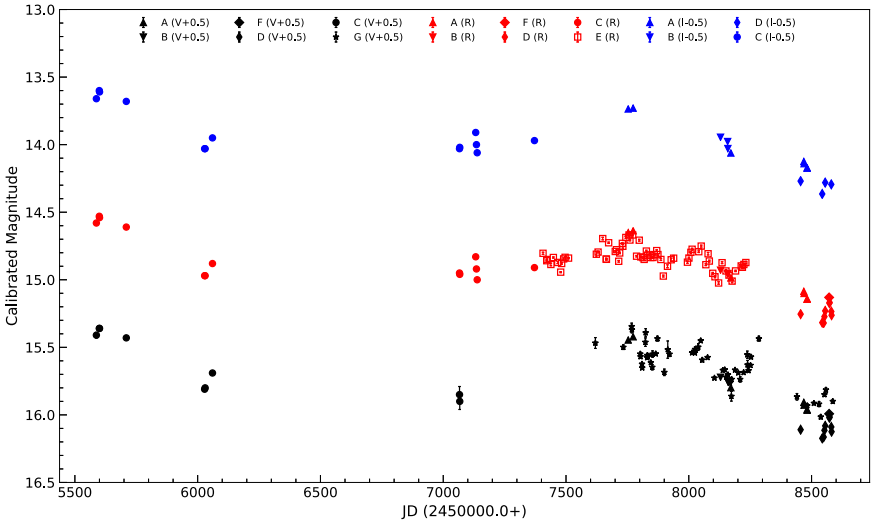

Figure 2. Long-term variability optical (*VRI*) light curves of 1ES 0806+524; these are shown in black (*V*), red (*R*), and blue (*I*).

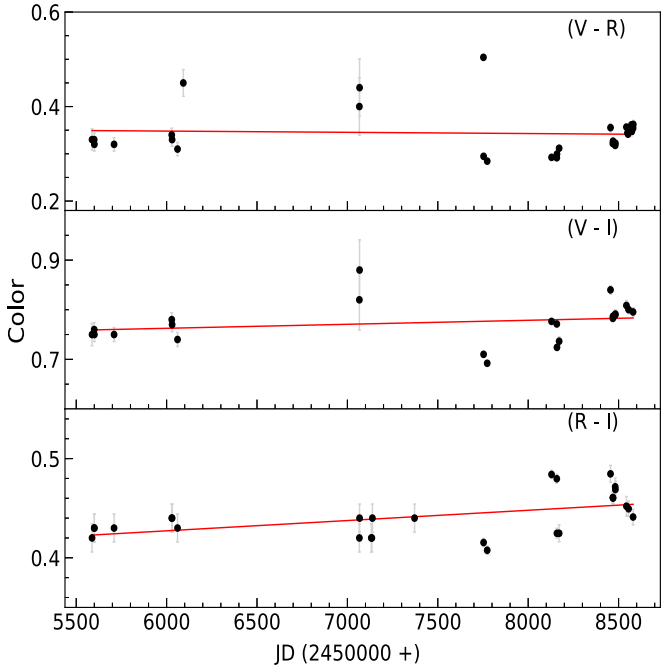

Figure 3. Optical color variations of 1ES 0806+524 with time during the entire monitoring period.

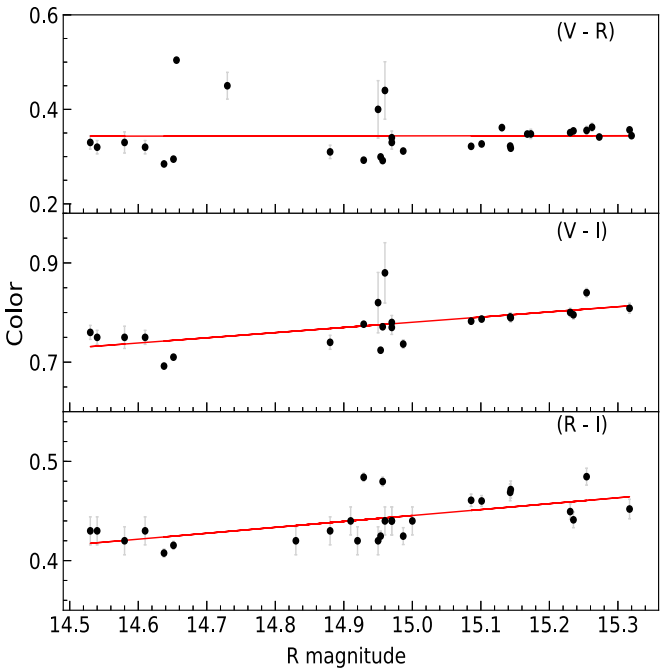

Figure 4. Optical color variations of 1ES 0806+524 against *R* magnitude.

hole. Hence, for blazars, jet-based theoretical models are mostly used to explain variations at all observable frequencies occurring on different timescales (e.g., Marscher & Gear 1985; Wagner & Witzel 1995). However, when the blazar is in its very low state and the jet may be very weak, the thermal emission from the AD can dominate over the nonthermal jet emission. In such cases, the microvariability in the LCs of blazars might be attributed to instabilities in the AD or eclipsing of the hotspots on the AD (e.g., Chakrabarti & Wiita 1993; Mangalam & Wiita 1993).

There are several possible explanations for brightness variations on STV/LTV timescales in the LCs of blazars. Propagation of a shock in the relativistic jet that accelerates electrons to high energies followed by subsequent cooling via synchrotron and inverse-Compton radiations, the basic shock-in-jet model, (e.g., Marscher & Gear 1985), can nicely explain most large flares. Many other changes can be understood to arise from small variations in the viewing angle, and hence in the Doppler factor, caused by either wiggling or helical jets or the motion of the most intense

Table 4
Variation of Color Indices with Respect to Time on LTV Timescales

Color Index	m_1[a]	c_1[a]	r_1[a]	p_1[a]
V–R	$-2.592e-06 \pm 7.807e-06$	0.364	−0.062	7.423e-01
V–I	$8.064e-06 \pm 7.542e-06$	0.714	0.227	2.971e-01
R–I	$1.035e-05 \pm 3.438e-06$	0.365	0.516	5.892e-03

Note.
[a] m_1 = slope and c_1 = intercept of CI against time; r_1 = Correlation coefficient; p_1 = null hypothesis probability.

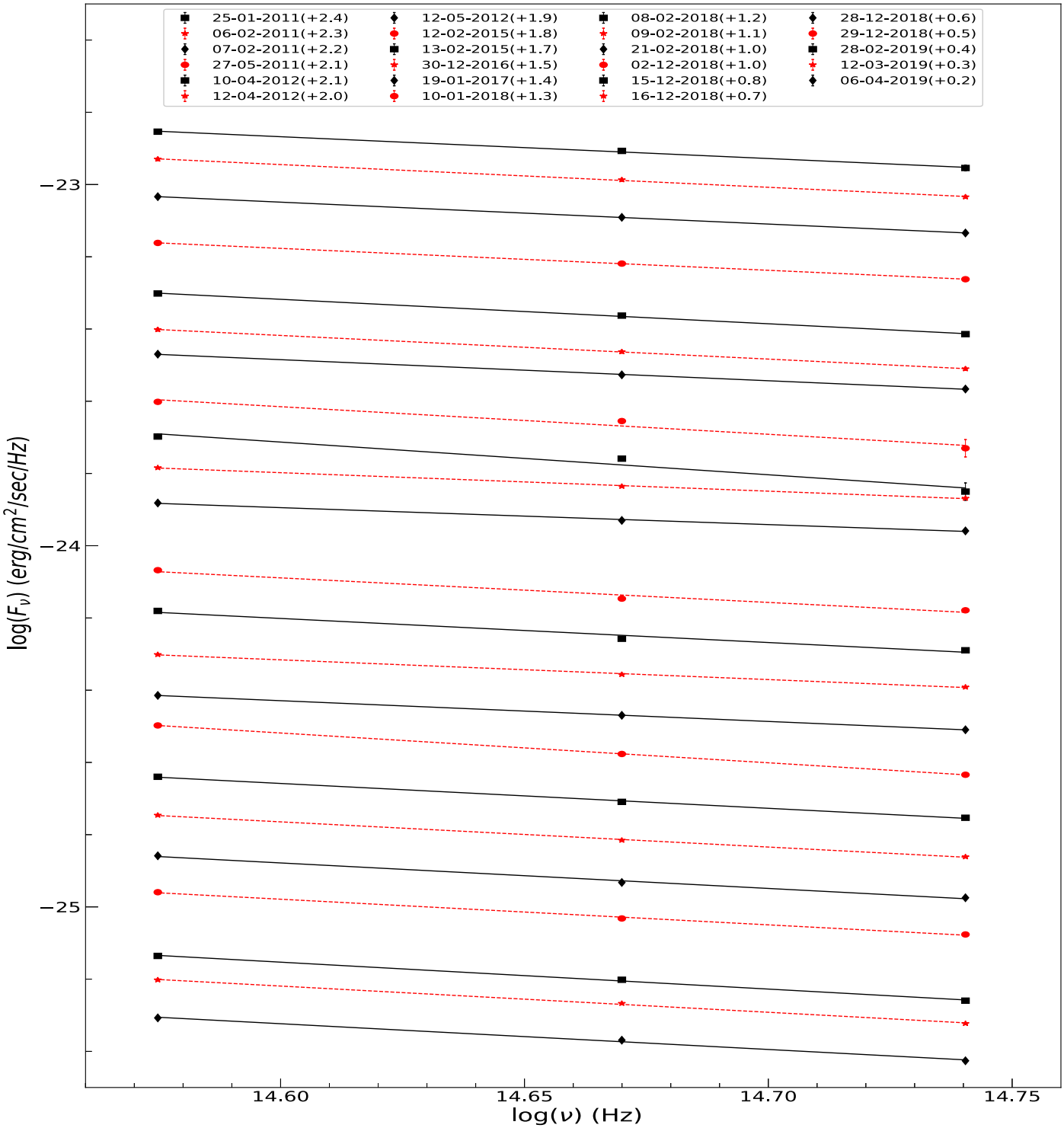

Figure 5. Spectal energy distributions of 1ES 0806+524 in *V*, *R*, and *I* bands.

emitting region on a roughly helical trajectory within the jet (e.g., Camenzind & Krockenberger 1992; Gopal-Krishna & Wiita 1992; Villata & Raiteri 1999). Variations on shorter (IDV) timescales can be explained by the turbulence expected in a relativistic plasma jet (e.g., Marscher 2014; Calafut & Wiita 2015; Pollack et al. 2016).

Observations at optical bands have suggested that the amplitude of flux variations on IDV timescales in the LCs of HBLs is significantly lower than that in the LCs of LBLs (e.g., Heidt & Wagner 1998; Romero et al. 1999; Gopal-Krishna et al. 2011). Our optical IDV results are consistent with this conclusion, as we found almost no statistically significant optical IDV in our many LCs of the TeV HBL 1ES 0806+524. Romero et al. (1999) suggested that the difference in the optical microvariability behavior of HBLs and LBLs could be due to the presence of stronger magnetic fields in HBLs. An axial magnetic field B can prevent the formation of Kelvin–Helmholtz instabilities in the bases of jets if its value exceeds

Table 5
Variation of Color Indices with Respect to *R* Magnitude on LTV Timescales

Color Index	m_2[a]	c_2[a]	r_2[a]	p_2[a]
V–*R*	$1.261e-03 \pm 3.580e-02$	0.325	0.007	9.721e-01
V–I	$1.045e-01 \pm 3.008e-02$	−0.787	0.604	2.276e-03
R–I	$5.965e-02 \pm 1.543e-02$	−0.449	0.612	6.999e-04

Note.
[a] m_2 = slope and c_2 = intercept of CI against *R* magnitude; r_2 = Correlation coefficient; p_2 = null hypothesis probability.

Table 6
Straight-line Fits to Optical SEDs of TeV Blazar 1ES 0806+524

Observation date	α[a]	C[a]	r_3[a]	p_3[a]
2011 Jan 25	0.604 ± 0.031	−14.047	−0.999	3.308e-02
2011 Feb 6	0.629 ± 0.020	−13.757	−1.000	1.986e-02
2011 Feb 7	0.607 ± 0.004	−14.193	−1.000	3.920e-03
2011 May 27	0.607 ± 0.004	−14.321	−1.000	3.920e-03
2012 Apr 10	0.677 ± 0.024	−13.430	−0.999	2.233e-02
2012 Apr 12	0.654 ± 0.008	−13.862	−1.000	7.647e-03
2012 May 12	0.584 ± 0.012	−14.962	−1.000	1.327e-02
2015 Feb 12	0.764 ± 0.143	−12.466	−0.983	1.177e-01
2015 Feb 13	0.905 ± 0.183	−10.498	−0.980	1.269e-01
2016 Dec 30	0.512 ± 0.020	−16.323	−0.999	2.454e-02
2017 Jan 19	0.469 ± 0.027	−17.046	−0.998	3.649e-02
2018 Jan 10	0.680 ± 0.104	−14.164	−0.989	9.629e-02
2018 Feb 8	0.667 ± 0.100	−14.466	−0.989	9.495e-02
2018 Feb 9	0.546 ± 0.023	−16.344	−0.999	2.690e-02
2018 Feb 21	0.575 ± 0.003	−16.041	−1.000	3.549e-03
2018 Dec 2	0.825 ± 0.004	−12.480	−1.000	3.086e-03
2018 Dec 15	0.688 ± 0.030	−14.615	−0.999	2.747e-02
2018 Dec 16	0.697 ± 0.022	−14.581	−1.000	1.967e-02
2018 Dec 28	0.706 ± 0.049	−14.572	−0.998	4.450e-02
2018 Dec 29	0.710 ± 0.038	−14.616	−0.999	3.399e-02
2019 Feb 28	0.745 ± 0.036	−14.275	−0.999	3.063e-02
2019 Mar 12	0.726 ± 0.030	−14.624	−0.999	2.602e-02
2019 Apr 6	0.713 ± 0.045	−14.915	−0.998	4.010e-02

Note.
[a] α = spectral index and C = intercept of $\log(F_\nu)$ against $\log(\nu)$; r_3 = Correlation coefficient; p_3 = null hypothesis probability.

the critical value B_c given by (Romero 1995)

$$B_c = [4\pi n_e m_e c^2(\Gamma^2 - 1)]^{1/2}\Gamma^{-1}, \quad (3)$$

where n_e is the local electron density, m_e is the electron rest mass, and Γ is the bulk Lorentz factor of the jet flow. In HBLs, such as in 1ES 0806+524, higher magnetic fields ($B > B_c$) would prevent the formation of small-scale structures that could produce microvariability or IDV in their optical LCs.

On LTV timescales, we found variations at all three optical frequencies; the amplitude of variability increases with increasing frequency. Our result is consistent with earlier studies (e.g., Papadakis et al. 2003; Gaur et al. 2015). This can be explained by the shock-in-jet model: the electrons accelerated at the shock front suffer energy losses via synchrotron radiation (Marscher & Gear 1985). The highest-energy electrons radiate faster than the lower-energy electrons and so emit radiation within a thin region behind the shock front. The thickness of the emitting region increases as the frequency decreases. Therefore, at higher frequencies the variability amplitude is higher and the variability timescale is shorter.

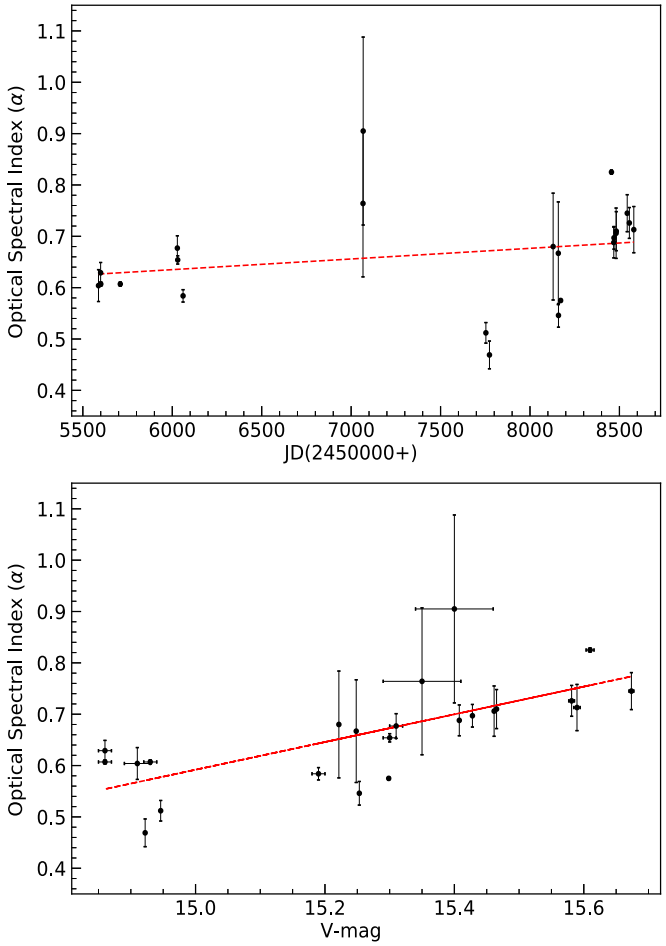

Figure 6. Variation of optical spectral index with respect to time (top) and *V*-band magnitude (bottom).

Table 7
Variation of Optical Spectral Index, α, with Respect to Time and *V*-band Magnitude during our Observing Campaign of 1ES 0806+524

Parameter	m_4[a]	c_4[a]	r_4[a]	p_4[a]
α versus time	$2.075e-05 \pm 1.763e-05$	0.511	0.249	2.523e-01
α versus *V*-mag	0.270 ± 0.060	−3.454	0.700	1.994e-04

Note.
[a] m_4 = slope and c_4 = intercept of α against time or *V*-magnitude; r_4 = Correlation coefficient; p_4 = null hypothesis probability.

In blazars, flux variations are often linked to changes in color. Blazars generally show one of two different color behaviors: a BWB or an RWB trend. BL Lac objects usually follow a BWB trend, while an RWB trend is generally observed in FSRQs (e.g., Gaur et al. 2012b, 2015). However, no clear trend in color variation has been reported in some blazars (e.g., Böttcher et al. 2009; Poon et al. 2009). It even has been found that the same source can simultaneously evince both these color behaviors when different pairs of filters are used to compute the colors (Wu et al. 2011). In the present

work, the HBL 1ES 0806+524 shows a BWB trend on LTV timescales. The BWB chromatism may indicate the presence of two components contributing to the overall optical emission: one variable component with a flatter slope and the other stable component with a steeper slope (Fiorucci et al. 2004).

6. Summary

In this study, we have presented the optical (*VRI*) photometric observations of the TeV HBL 1ES 0806+524 taken with seven ground-based telescopes on 153 nights between 2011 January 25 and 2019 April 12. The results we obtained are summarized below.

1. No clearly significant intraday variation was observed in any optical band LC during 17 of 18 nights and it was very weak on that remaining night.
2. We found no variations in $V-R$ color with time on IDV timescales.
3. On LTV timescales, flux variations were seen in all three optical (V, R, and I) bands. The variability amplitudes were 84.3%, 81.6%, and 76.5% in V, R, and I bands, respectively.
4. There were modest color variations over this eight year span of observations. Only the $R-I$ color showed a detectable trend over time, while there were significant correlations of $V-I$ and $R-I$ colors with brightness.
5. No systematic temporal variation was found in the spectral index, while the optical spectral index was significantly correlated with the V-band magnitude.

This study concludes that, at optical frequencies, the TeV HBL 1ES 0806+524 shows almost no statistically significant variation on IDV timescales, while on longer timescales it exhibits large flux variations and follows the general BWB trend seen for HBLs. It has rather steep optical spectra, with a mean spectral index of 0.639 ± 0.002, consistent with synchrotron emission dominating the optical light and with the presence of relatively strong axial magnetic fields in the jet.

We thank the anonymous referee for useful comments and suggestions that helped us in improving our manuscript. S.O.K. acknowledges financial support by Shota Rustaveli National Science Foundation of Georgia under contract PHDF-18-354. The Abastumani team acknowledges financial support by the Shota Rustaveli National Science Foundation of Georgia under contract FR/217554/16. J.Z. acknowledges support from National Natural Science Foundation of China (grants No. 11973050 and 11573034). The Bulgarian team acknowledges support from the Bulgarian NSF through grants DN08-1/2016, DN 18-13/2017, DN 18-10/2017, KP-06-H28/3 (2018), and KP-06-PN38/4 (2019). G.D. and O.V. acknowledge observing grant support from the Institute of Astronomy and Rozhen National Astronomical Observatory, Bulgarian Academy of Sciences, through the bilateral joint research project "Study of ICRF radio-sources and fast variable astronomical objects" (for the period 2017-2019, head—G. Damljanovic). This work is a part of the project No. 176011 "Dynamics and kinematics of celestial bodies and systems," No. 176004 "Stellar physics" and No. 17021 "Visible and invisible matter in nearby galaxies: theory and observations" supported by the Ministry of Education, Science and Technological Development of the Republic of Serbia.

Software: IRAF (http://iraf.net), DAOPHOT II (Stetson 1987, 1992), python 2.7 (http://www.python.org).

ORCID iDs

Ashwani Pandey https://orcid.org/0000-0003-3820-0887
Alok C. Gupta https://orcid.org/0000-0002-9331-4388
Paul J. Wiita https://orcid.org/0000-0002-1029-3746
E. Semkov https://orcid.org/0000-0002-1839-3936

References

Abdo, A. A., Ackermann, M., Agudo, I., et al. 2010, ApJ, 716, 30
Acciari, V., Aliu, E., Arlen, T., et al. 2009, ApJL, 690, L126
Aleksić, J., Ansoldi, S., Antonelli, L. A., et al. 2015, MNRAS, 451, 739
Bade, N., Beckmann, V., Douglas, N. G., et al. 1998, A&A, 334, 459
Böttcher, M. 2007, Ap&SS, 307, 69
Böttcher, M., Fultz, K., Aller, H. D., et al. 2009, ApJ, 694, 174
Calafut, V., & Wiita, P. J. 2015, JApA, 36, 255
Camenzind, M., & Krockenberger, M. 1992, A&A, 255, 59
Carini, M. T. 1990, PhD thesis, Georgia State Univ.
Chakrabarti, S. K., & Wiita, P. J. 1993, ApJ, 411, 602
Ciprini, S., Tosti, G., Raiteri, C. M., et al. 2003, A&A, 400, 487
de Diego, J. A. 2014, AJ, 148, 93
de Diego, J. A., Polednikova, J., Bongiovanni, A., et al. 2015, AJ, 150, 44
Fiorucci, M., Ciprini, S., & Tosti, G. 2004, A&A, 419, 25
Fossati, G., Maraschi, L., Celotti, A., Comastri, A., & Ghisellini, G. 1998, MNRAS, 299, 433
Gaur, H., Gupta, A. C., Bachev, R., et al. 2015, MNRAS, 452, 4263
Gaur, H., Gupta, A. C., Strigachev, A., et al. 2012a, MNRAS, 420, 3147
Gaur, H., Gupta, A. C., Strigachev, A., et al. 2012b, MNRAS, 425, 3002
Gopal-Krishna, Goyal, A., Joshi, S., et al. 2011, MNRAS, 416, 101
Gopal-Krishna, & Wiita, P. J. 1992, A&A, 259, 109
Gupta, A. C., Agarwal, A., Bhagwan, J., et al. 2016, MNRAS, 458, 1127
Gupta, A. C., Banerjee, D. P. K., Ashok, N. M., & Joshi, U. C. 2004, A&A, 422, 505
Gupta, A. C., Gaur, H., Wiita, P. J., et al. 2019, AJ, 157, 95
Heidt, J., & Wagner, S. J. 1996, A&A, 305, 42
Heidt, J., & Wagner, S. J. 1998, A&A, 329, 853
Kshama, S. K., Paliya, V. S., & Stalin, C. S. 2017, MNRAS, 466, 2679
Kurtanidze, O. M., Tetradze, S. D., Richter, G. M., et al. 2009, in ASP Conf. Ser. 408, The Starburst–AGN Connection, ed. W. Wang et al. (San Francisco, CA: ASP), 266
Man, Z., Zhang, X., Wu, J., Zhou, X., & Yuan, Q. 2014, AJ, 148, 110
Mangalam, A. V., & Wiita, P. J. 1993, ApJ, 406, 420
Marcha, M. J. M., Browne, I. W. A., Impey, C. D., & Smith, P. S. 1996, MNRAS, 281, 425
Marscher, A. P. 2014, ApJ, 780, 87
Marscher, A. P., & Gear, W. K. 1985, ApJ, 298, 114
Miller, H. R., Carini, M. T., & Goodrich, B. D. 1989, Natur, 337, 627
Padovani, P., Alexander, D. M., Assef, R. J., et al. 2017, A&ARv, 25, 2
Pandey, A., Gupta, A. C., Wiita, P. J., & Tiwari, S. N. 2019, ApJ, 871, 192
Papadakis, I. E., Boumis, P., Samaritakis, V., & Papamastorakis, J. 2003, A&A, 397, 565
Polednikova, J., Ederoclite, A., de Diego, J. A., et al. 2016, MNRAS, 460, 3950
Pollack, M., Pauls, D., & Wiita, P. J. 2016, ApJ, 820, 12
Poon, H., Fan, J. H., & Fu, J. N. 2009, ApJS, 185, 511
Rees, M. J. 1984, ARA&A, 22, 471
Reinthal, R., Lindfors, E. J., Mazin, D., et al. 2012, JPhCS, 355, 012017
Romero, G. E. 1995, Ap&SS, 234, 49
Romero, G. E., Cellone, S. A., & Combi, J. A. 1999, A&AS, 135, 477
Schachter, J. F., Stocke, J. T., Perlman, E., et al. 1993, ApJ, 412, 541
Stetson, P. B. 1987, PASP, 99, 191
Stetson, P. B. 1992, in ASP Conf. Ser. 25, Astronomical Data Analysis Software and Systems I, ed. D. M. Worrall, C. Biemesderfer, & J. Barnes (San Francisco, CA: ASP), 297
Stocke, J. T., Morris, S. L., Gioia, I. M., et al. 1991, ApJS, 76, 813
Urry, C. M., & Padovani, P. 1995, PASP, 107, 803
Villata, M., & Raiteri, C. M. 1999, A&A, 347, 30
Wagner, S. J., & Witzel, A. 1995, ARA&A, 33, 163
Wierzcholska, A., Ostrowski, M., Stawarz, Ł., Wagner, S., & Hauser, M. 2015, A&A, 573, A69
Wu, J., Böttcher, M., Zhou, X., et al. 2012, AJ, 143, 108
Wu, J., Zhou, X., Ma, J., & Jiang, Z. 2011, MNRAS, 418, 1640